AIP | Journal of Applied Physics

Fabrication and photoluminescence of ZnS:Mn2+ nanowires/ZnO quantum dots/SiO2 heterostructure

Jinghai Yang, Jian Cao, Lili Yang, Yongjun Zhang, Yaxin Wang et al.

Citation: J. Appl. Phys. 108, 044304 (2010); doi: 10.1063/1.3467762
View online: http://dx.doi.org/10.1063/1.3467762
View Table of Contents: http://jap.aip.org/resource/1/JAPIAU/v108/i4
Published by the American Institute of Physics.

Fabrication and photoluminescence of ZnS:Mn^{2+} nanowires/ZnO quantum dots/SiO_2 heterostructure

Jinghai Yang,[1,a)] Jian Cao,[1,2] Lili Yang,[1] Yongjun Zhang,[1] Yaxin Wang,[1] Xiaoyan Liu,[1] Dandan Wang,[2] Maobin Wei,[1] Ming Gao,[1] and Jihui Lang[1]

[1]*Institute of Condensed State Physics, Jilin Normal University, Siping 136000, People's Republic of China and Key Laboratory of Functional Materials Physics and Chemistry, Jilin Normal University, Siping 136000, People's Republic of China*

[2]*Key Laboratory of Excited State Physics, Changchun Institute of Optics, Fine Mechanics and Physics, Chinese Academy of Sciences, 3888 Eastern Nan-Hu Road, Changchun 130033, People's Republic of China and Graduate School of Chinese Academy of Sciences, Beijing 100049, People's Republic of China*

(Received 28 March 2010; accepted 28 June 2010; published online 18 August 2010)

In this paper, we demonstrated the encapsulation of ZnS:Mn^{2+} nanowires (NWs) and ZnO quantum dots (QDs) with a layer of mesoporous SiO_2 shell for the purpose of integrating dual emission property into one common nanostructure. The average diameter of ZnS:Mn^{2+} NWs, ZnO QDs, and ZnS:Mn^{2+}/ZnO@SiO_2 heterostructure was about 10 nm, 6 nm, and 22 nm, respectively. Within ZnS:Mn^{2+}/ZnO@SiO_2 nanocomposites, the intensity of the yellow-orange emission contributed by ZnS:Mn^{2+} NWs and the UV emission contributed by ZnO QDs was three and ten times higher than their individual components, respectively. The fluorescence intensity ratio of the dual emission can be tuned by adjusting the hydrolysis time of tetraethyl orthosilicate. The peak energy of the yellow-orange and UV emission showed blueshift and redshift as increasing the temperature, respectively. The anomalous enhancement of the integrated intensity for the UV emission with the temperature indicated that the high surface state density existing in ZnO QDs can overrun the influence of temperature quenching and even alter the photoluminescent properties. © *2010 American Institute of Physics*. [doi:10.1063/1.3467762]

I. INTRODUCTION

Semiconductor heterostructures with modulated compositions can integrate several different functions into one integrated nanostructure on the requirement of some certain applications, which are essential for developing potential nanoelectronic and optoelectronic devices.[1,2] Various types of heterostructures, such as core-sheath coaxial nanostructures, bicoaxial nanowires (NWs) and semiconductor-metal nanostructures, have been reported.[3–5] Recently, new heterostructures, i.e., the core-shell structures with different shape and content, have attracted considerable attention. For example, Song *et al.*[6] encapsulated CdTe quantum dots (QDs) and ZnO nanorods into a layer of mesoporous SiO_2 shell, which exhibited bioluminescent properties and ultrasensitive fluorescence response to metal ions. Yang *et al.*[7] reported branched heterostructures consisted of ZnO stems and Zn_3P_2 branches, exhibiting highly efficient spatially resolved photodetector characteristics.

ZnO (Eg=3.37 eV at 300 K) and ZnS (Eg=3.77 eV at 300 K), well-known direct band gap II–VI semiconductors, are promising materials for fabricating photonic, optical, and electronic devices.[8–10] Recent progress in the synthesis of highly monodispersed ZnO and ZnS nanocrystallites have paved the way for numerous spectroscopy studies on the ZnO/ZnS heterostructures from both experimental and theoretical points of view. So far, the ZnO/ZnS heterostructures, such as biaxial nanobelt,[11] nanoribbons,[12] nanotetrapods,[13] NWs (Ref. 14) have been successfully synthesized and studied. To further improve the properties of ZnS/ZnO heterostructures, we are trying to dope other elements into the system. It is well known that the divalent Mn^{2+} ions are appropriate dopants for these II–VI group semiconductor materials since Mn doping cannot only enhance their optical transition efficiency and increase the number of the luminescent centers but also inspire them to exhibit interesting magneto-optical properties.[15–17] Upon excitation, the Mn^{2+} doped ZnS nanostructures would produce characteristic bright yellow-orange emission (~585 nm) due to the $^4T_1-^6A_1$ transition of Mn^{2+}.[18] For ZnO, the excitonic emission (~380 nm at room temperature) is desirable due to its promising application in various UV nanodevices. Whereas, the visible emission (400–700 nm) is usually not expected because it depends on the species of defects and the concentration of each kind of defects so that its intensity and position are not easily manipulated. Consequently, if ZnS:Mn^{2+} with controllable yellow-orange emission can be combined with ZnO with pure excitonic emission, the system of ZnS:Mn^{2+}/ZnO will exhibit both tunable visible emission and UV emission, which should be superior to other organic and complex materials with dual emissions. To improve the reliability and stability of the ZnS:Mn^{2+}/ZnO system, the silica coating has been utilized in our experiments since it has been proved to be an ideal protection method for nanocrystals. Usually, silica shell is chemically inert and optical transparent, so it is a feasible and effective way to avoid uncontrollable surface effect, thus improving the reliability and long-term stability of the devices. Therefore, in prin-

[a)]Electronic mail: jhyang1@jlnu.edu.cn.

ciple, the $ZnS:Mn^{2+}/ZnO$ system passivated by SiO_2 shell, i.e., $ZnS:Mn^{2+}/ZnO@SiO_2$ would exhibit good photostability and high luminescent efficiency.

In this paper, we present, for the first time as well as we known, the fabrication of a novel $ZnS:Mn^{2+}$ NWs/ZnO QDs @ SiO_2 core-shell heterostructures. We not only provide the simple preparation method but also investigate the photoluminescent (PL) properties of $ZnS:Mn^{2+}$ NWs, ZnO QDs, and $ZnS:Mn^{2+}/ZnO/SiO_2$ heterostructures in detail. We hope that our results can stimulate more fabrication and study of innovative semiconductor heterostructures with various compositions and shapes to obtain unique properties.

II. EXPERIMENTS

A. Materials

Zinc nitrate, zinc chloride, manganese nitrate, thiourea, ammonium bicarbonate, sodium dodecyl sulfate (SDS), cetyltrimethylammonium bromide (CTAB), tetraethyl orthosilicate (TEOS), and ethylenediamine (EN) are all analytical grade (Shanghai Chemical Reagents Co.) and used without further purification.

B. Synthesis of $ZnS:Mn^{2+}$ (1%) NWs (Ref. 19)

In a typical process, 0.99 mmol of zinc nitrate and 0.01 mmol of manganese nitrate were dissolved in 16 ml EN and water (1:1 in volume ratio). After stirring for 1 h, 3 mmol of thiourea were put into the resulting complex. After stirring for 2 h, the colloid solution was transferred into a 20 ml Teflon-lined autoclave and kept at 180 °C for 12 h. After the reaction, the autoclave was taken out and cooled down to room temperature. The product was washed with ethanol and deionized water for several times and separated by centrifugation, and then dried at 80 °C for 1 h to get a white powder.

C. Synthesis of ZnO QDs (Ref. 20)

40 ml of aqueous solutions of ammonium bicarbonate (1 mol/l) and 12.5 μl of aqueous solutions of SDS (1 mol/l) were first mixed together in one beaker. Under constant magnetic stirring, 25 ml of aqueous solutions of zinc chloride (1 mol/l) was added slowly (dropwise for 10 min) into the resulting solution. During the dropping process, the white precipitations were gradually formed in the solution. After 2 h reaction, the product was filtered and washed with anhydrous ethanol several times to remove the impurities, followed by drying in an oven for 4 h at 50 °C. Finally, ZnO QDs with a light yellow color were obtained after annealing the precursors in air under 200 °C for 1 h in the chamber furnace.

D. Synthesis of $ZnS:Mn^{2+}/ZnO@SiO_2$ core/shell nanostructures (Ref. 6)

In a typical process, 50 ml of absolute alcohol, 1 ml of distilled water, 1.7 ml of aqueous ammonia, and 200 μl of TEOS were injected into a 100 ml conical flask. This mixed solution was stirred for 10 min at room temperature. After that, $ZnS:Mn^{2+}$ (1%) NWs (0.008 g), ZnO QDs (0.035 g), and CTAB (0.1 g) dispersed ultrasonically in distilled water (10 ml) were added to the foregoing solution. The mixture was continuously stirred for 6 h at room temperature. The resulting ternary nanocomposites consisting of SiO_2, $ZnS:Mn^{2+}$ NWs, and ZnO QDs were then isolated by centrifugation and washed with hot deionized water to remove excess QDs as well as CTAB as much as possible. For each washing, the ultrasonic technique was used to entirely disperse the nanoparticles in water. To obtain an optimized time for surface capping, a set of samples were synthesized at different time periods (t=0.5, 1.5, 3, 9, 12 h).

E. Characterization of products

X-ray diffraction (XRD) patterns were collected on a MAC Science MXP-18 X-ray diffractometer using a Cu target radiation source. Transmission electron micrographs (TEM) and high-resolution transmission electron microscopy (HRTEM) images were taken on JEM-2100 electron microscope. The specimen was prepared by depositing a drop of the dilute solution of the sample in 2-propanol on a carbon-coated copper grid and drying at room temperature. Fourier transform infrared (FT-IR) spectra were recorded on a Bruker Vertex 70 spectrophotometer in KBr pellets. X-ray photoelectron spectra (XPS) were recorded on a Vgescalab MK II XPS using Mg $K\alpha$ radiation ($h\upsilon$=1253.6 eV) with a resolution of 1.0 eV. UV-vis absorption spectra were measured on an UV-3101PC UV spectrometer. The specimen for the measurement was dispersed in ethanol and placed in a 1 cm quartz cell, and ethanol served as the reference. PL measurement was carried out at room temperature, using 325 nm as the excitation wavelength, He–Cd laser as the source of excitation. In the measurements of the temperature-dependent PL, the specimen was put into a liquid nitrogen cycling system, in which the temperature varied in the range of 77–300 K. A continuous 325 nm light of a He–Cd laser was used as the excitation source.

III. RESULTS AND DISCUSSIONS

A. Structure and morphology of $ZnS:Mn^{2+}/ZnO@SiO_2$ core/shell nanostructures

Figure 1 shows the structure and morphology of the initial $ZnS:Mn^{2+}$ NWs and ZnO QDs for preparing the core-shell nanocomposites. As seen from the XRD pattern of $ZnS:Mn^{2+}$ NWs [Fig. 1(a)], all the diffraction peaks can be well indexed as ZnS with hexagonal wurtzite structure, which is consistent with the standard card [Joint Committee for Powder Diffraction Standard (JCPDS) No. 36-1450]. It is noticeable that the (002) diffraction peak is stronger and narrower than the other peaks, suggesting a preferential growth direction along the c-axis.[21] Figure 1(b) shows that the $ZnS:Mn^{2+}$ NWs are smooth and uniform over their entire lengths and the average diameter is about 10 nm. The HR-TEM image [see inset of Fig. 1(b)] corresponding to the region marked by a red dot box in Fig. 1(b) further proves that the NWs grow along the (002) direction, which exhibits a well oriented and good crystallization. Figure 1(c) displays the XRD pattern of ZnO QDs. It can be seen that all the diffraction peaks can be indexed as ZnO with hexagonal

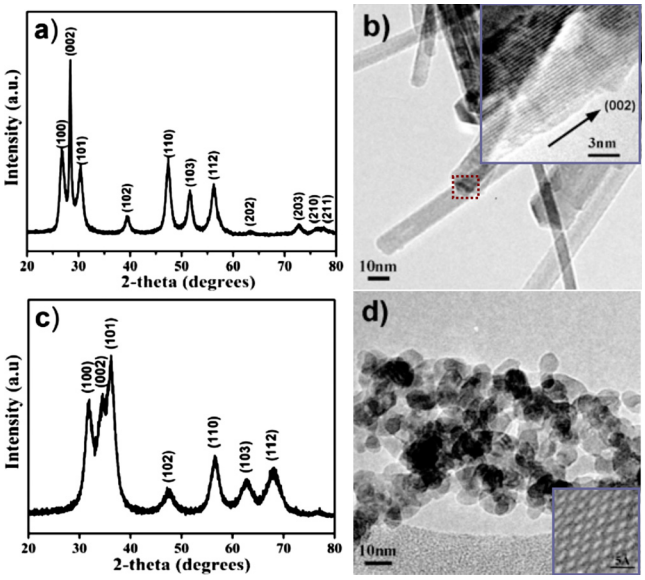

FIG. 1. (Color online) (a) and (b) XRD pattern and TEM image of $ZnS:Mn^{2+}$ NWs. (c) and (d) XRD pattern and TEM image of ZnO QDs. The inset of (b) and (d) show the HRTEM images of $ZnS:Mn^{2+}$ NWs and ZnO QDs, respectively.

wurtzite structure, which is consistent with the standard card (JCPDS No. 800075). Figure 1(d) shows that the average diameter of the QDs is about 6 nm. The HRTEM image of ZnO QDs [see inset of Fig. 1(d)] shows that these QDs are well crystallized.

Figure 2 display the TEM and HRTEM images of $ZnS:Mn^{2+}/ZnO@SiO_2$ nanocomposites. As can be seen from the TEM image [Fig. 2(a)], the dark contrast corresponding to $ZnS:Mn^{2+}/ZnO$ has a diameter of about 20 nm. Compared with $ZnS:Mn^{2+}$ NWs [Fig. 1(b)], the diameter of the dark contrast increase, and its surface is not smooth, demonstrating that ZnO QDs exist on the surface of $ZnS:Mn^{2+}$ NWs. Whereas, the light contrast sheath in Fig. 2(a) corresponding to SiO_2 has a thickness of about 2 nm,

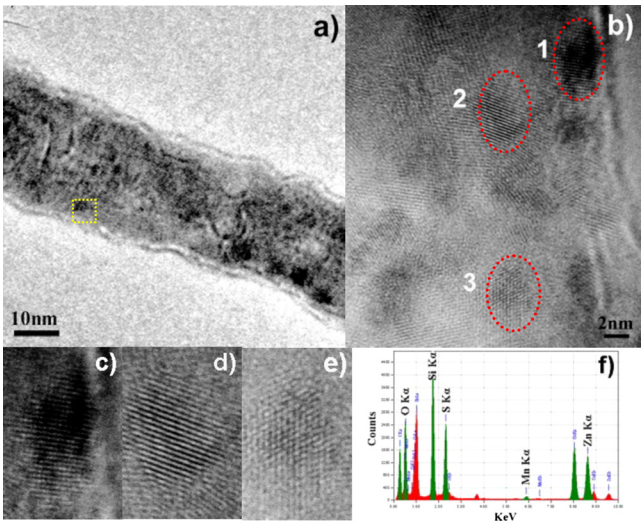

FIG. 2. (Color online) (a) and (b) TEM and HRTEM images of $ZnS:Mn^{2+}/ZnO@SiO_2$ nanocomposites. [(c)–(e)] The enlarged images of the oval region 1, 2, and 3 in Fig. 2(b). (f) EDS image of $ZnS:Mn^{2+}/ZnO@SiO_2$ nanocomposites.

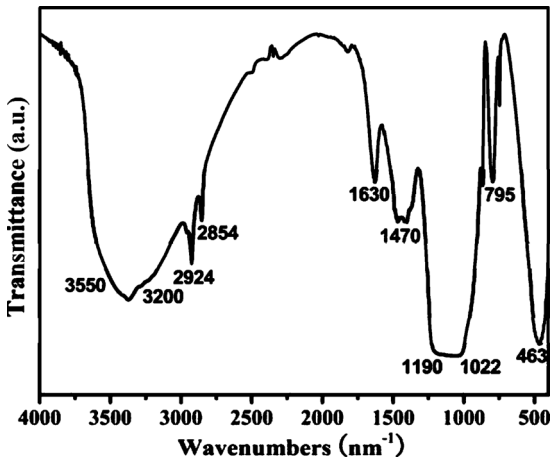

FIG. 3. FT-IR spectrum of $ZnS:Mn^{2+}/ZnO@SiO_2$ nanocomposites.

which indicates that $ZnS:Mn^{2+}$ NWs and ZnO QDs are successfully embedded within the SiO_2 matrix. The HRTEM image [Fig. 2(b)] of $ZnS:Mn^{2+}/ZnO@SiO_2$ nanocomposites corresponding to the region marked by a yellow dot box in Fig. 2(a) also exhibits the core-shell feature of the nanocomposites since ZnO QDs on the surface of $ZnS:Mn^{2+}$ NWs can be observed clearly. The enlarged images of the marked regions 1, 2, and 3 in Figs. 2(c)–2(e) show that these QDs are well crystallized, which are consistent with that of ZnO QDs [Fig. 1(d)]. Figure 2(f) shows the EDS spectrum of the nanocomposites, exhibiting the presence of the Zn, S, Mn, O, and Si element, which unambiguously confirms that the nanocomposites are composed of $ZnS:Mn^{2+}$ NWs, ZnO QDs, and SiO_2.

FT-IR analysis is an useful way to study the surface chemical structure of the sample. Figure 3 shows the FT-IR spectrum of $ZnS:Mn^{2+}/ZnO@SiO_2$ nanocomposites. The presence of the bands around 1190–1022 cm^{-1}, 795 cm^{-1}, and 463 cm^{-1} can be assigned to the Si–O–Si asymmetric stretching vibration, Si–O–Si symmetric stretching vibration, and Si–O–Si bend vibration,[22,23] respectively, which demonstrates the successfully coating SiO_2 on the surface of $ZnS:Mn^{2+}/ZnO$. In addition, the bands at about 3200–3550, 1470, and 1630 cm^{-1} can be assigned to the OH^- group on the nanocomposites surface.[22,24,25] The bands at 2800–3000 cm^{-1} can be assigned to the symmetric and asymmetric stretching vibrations of $-CH_2-$ and $-CH_3-$ groups, indicating the existence of CTAB.[22] The characteristic bands of Zn–O–Zn (at 620 or 816 cm^{-1})[24] and Zn–S–Zn (595–620 cm^{-1}) (Ref. 25) do not appear, illustrating the fact that $ZnS:Mn^{2+}/ZnO$ are covered by SiO_2.

XPS is a sensitive tool for the analysis of the surface chemical compositions of the sample. Figure 4 are the typical XPS spectra of the nanocomposites, where Fig. 4(a) is the survey spectrum and Figs. 4(b)–4(e) are the high-resolution XPS spectra for Si, O, Zn, and S species, respectively. The signals from Si, O, Zn, S elements can be found. Apparently, the signals of Si, O, and Zn arise from the components of SiO_2, $ZnS:Mn^{2+}$ NWs, and ZnO QDs, while the signal of S arises from the component of $ZnS:Mn^{2+}$ NWs. Since XPS cannot usually detect the Mn element in Mn doped ZnS nanostructures.[26] Here, the Mn peak is compa-

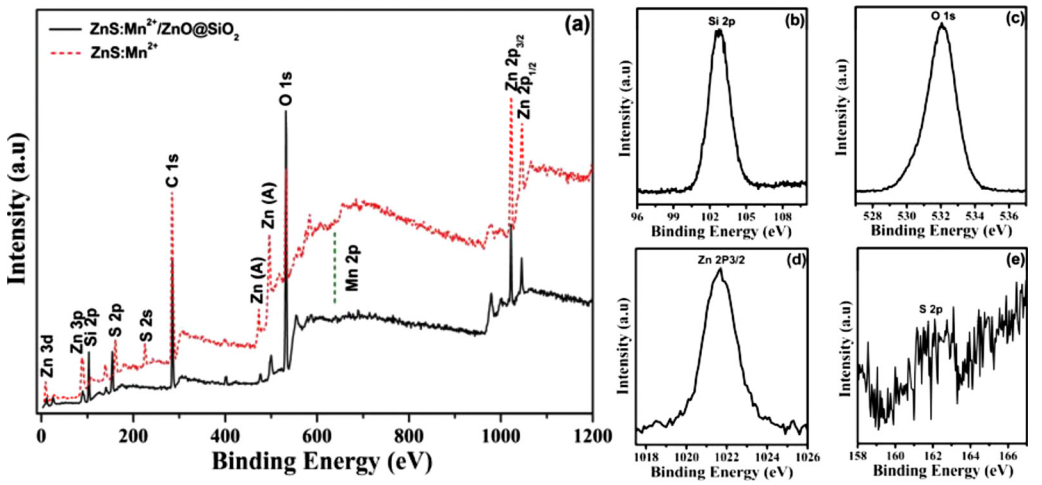

FIG. 4. (Color online) (a) XPS survey spectra of $ZnS:Mn^{2+}/ZnO@SiO_2$ nanocomposites (black line) and $ZnS:Mn^{2+}$ NWs (red dotted line). [(b)–(e)] The high-resolution XPS spectra of Si $2p$, O $1s$, Zn $2p$, and S $2p$ for $ZnS:Mn^{2+}/ZnO@SiO_2$ nanocomposites.

rable to the noise level, which is too weak to be detected. For $ZnS:Mn^{2+}/ZnO@SiO_2$ nanocomposites [black line in Figs. 4(a)], the signals of the Zn and S are weaker than that for $ZnS:Mn^{2+}$ NWs [red dotted line in Fig. 4(a)], demonstrating that $ZnS:Mn^{2+}$ NWs and ZnO QDs have been confined into one integrated nanostructure by SiO_2. In Figs. 4(b) and 4(c), we can observe the Si $2p$ peak at 102.7 eV (Ref. 27) and the O $1s$ peak at 532.1 eV,[28] corresponding to the standard binding energy of Si and O from SiO_2, which further confirms the SiO_2 covering on the surface of $ZnS:Mn^{2+}/ZnO$.

B. Optical properties of $ZnS:Mn^{2+}/ZnO@SiO_2$ core/shell nanostructures

Figures 5(a) and 5(b) shows the absorption spectrum of $ZnS:Mn^{2+}$ NWs and ZnO QDs, respectively. The absorption curve is smooth and the absorption peak is obtained at 315 nm (3.94 eV) for $ZnS:Mn^{2+}$ NWs [Fig. 5(a)] and 360 nm (3.45 eV) for ZnO QDs [Fig. 5(b)], respectively, both of which display blueshift compared to the bulk ZnS (3.77 eV) (Ref. 29) and ZnO (3.37 eV),[30] indicating the formation of nanomaterials. For $ZnS:Mn^{2+}/ZnO@SiO_2$ nanocomposites [Fig. 5(c)], a broad absorption band from 300 to 375 nm can be observed, which can also prove that both $ZnS:Mn^{2+}$ NWs and ZnO QDs are packed in SiO_2 matrix. The small redshift in the absorption peak position may be related to the increase in the nanocomposites size.

Figure 6 presents the room temperature PL spectra of $ZnS:Mn^{2+}$ NWs, ZnO QDs, and $ZnS:Mn^{2+}/ZnO@SiO_2$ nanocomposites. The PL spectrum of $ZnS:Mn^{2+}$ NWs [blue line (the second from the top curve)] shows a strong yellow-orange emission peak centered at 2.116 eV (corresponding to the Mn^{2+} $^4T_1-^6A_1$ transition) and a weak broad blue-green emission band (coming from the defect states emission: S vacancy, Zn vacancy and surface states[31,32]), indicating that the Mn^{2+} ions have been successfully incorporated into the ZnS lattice.[33] The PL spectrum of ZnO QDs [green line ×1 (the fourth from the top curve), ×5 (the third from the top curve)] consists of a weak UV peak centered at 3.26 eV and a broad strong deep level emission band in the range of 1.9–2.4 eV. The UV emission originates from the recombination of the free excitons in the near-band-edge and the deep level emission has commonly been attributed to the oxygen vacancies from ZnO.[34,35] After embedding $ZnS:Mn^{2+}$ NWs and ZnO QDs together within SiO_2 matrix [red line (the first

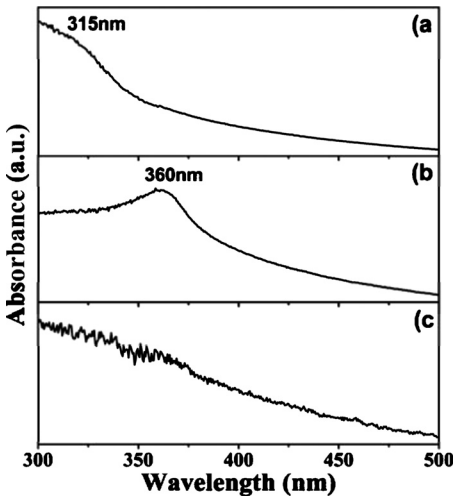

FIG. 5. UV-vis absorption spectra of (a) $ZnS:Mn^{2+}$ NWs, (b) ZnO QDs, and (c) $ZnS:Mn^{2+}/ZnO@SiO_2$ nanocomposites.

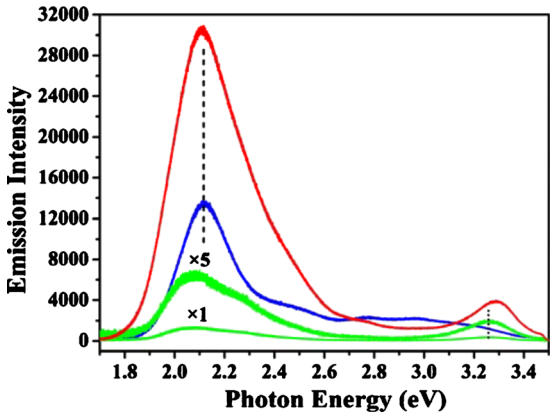

FIG. 6. (Color online) Room temperature PL spectra of $ZnS:Mn^{2+}$ NWs (blue line), ZnO QDs (green line), and $ZnS:Mn^{2+}/ZnO@SiO_2$ nanocomposites (red line).

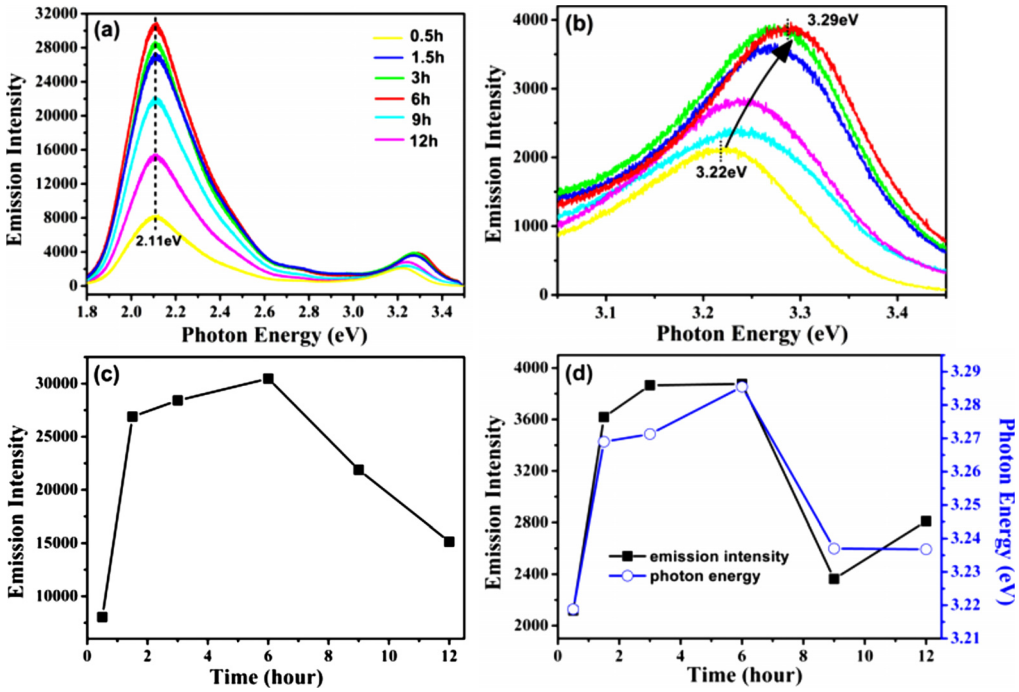

FIG. 7. (Color online) (a) Room temperature PL spectra of $ZnS:Mn^{2+}/ZnO@SiO_2$ nanocomposites with the growth time of 0.5, 1.5, 3, 6, 9, and 12 h. (b) The enlarged image of the UV emission in Fig. 7(a). (c) The intensity of the yellow-orange emission at different growth times. (d) The intensity and peak position of the UV emission at different growth times.

from the top curve)], it possesses yellow-orange emission and UV emission simultaneously, and the defect state emissions are greatly suppressed. The intensity of the yellow-orange and UV emission is three and ten times higher than their individual components, respectively, implying the high optical quality of the prepared $ZnS:Mn^{2+}/ZnO@SiO_2$ nanocomposites. In addition, the positions of the yellow-orange and UV emission are redshift (6 meV≈1.6 nm) and blueshift (30 meV≈3.5 nm), respectively. For $ZnS:Mn^{2+}$ NWs and ZnO QDs individually, the yellow-orange emission and UV emission would be affected by the surface effects, such as surface adsorption, existence of surface dangling bonds etc. When ZnO QDs absorbed on the surface of $ZnS:Mn^{2+}$ NWs, the energy transfer from the Mn^{2+} ions to the surface quenching centers was suppressed because of the increased distance from the Mn^{2+} ions to the surface of $ZnS:Mn^{2+}/ZnO$.[36] When SiO_2 coated on the surface of $ZnS:Mn^{2+}/ZnO$ nanocomposites, the O vacancies on the surface of ZnO QDs were decreased due to the formation of –O–Si–O– bond. As a result, the surface passivation would decrease the possibility of the nonradiative recombination caused by the surface states on the surface of $ZnS:Mn^{2+}$ NWs and ZnO QDs, so that $ZnS:Mn^{2+}/ZnO@SiO_2$ nanocomposites exhibit significantly enhanced PL intensity of the yellow-orange and UV emission. In addition, the localized strain and interface effect would also influence the optical properties of the core-shell nanomaterials.[37,38] Here, we suggest that the residual stress caused by the small lattice mismatch between $ZnS:Mn^{2+}$ NWs and ZnO QDs contribute to the slight redshift in the Mn^{2+} emission,[39] and the covalently bonding between ZnO and SiO_2 is primarily responsible for the blueshift in the UV emission.[22] Therefore, the as-prepared $ZnS:Mn^{2+}/ZnO@SiO_2$ nanocomposites are more applicable for the fabrication of optoelectronic devices, such as UV light-emitting diodes and diode lasers.

The PL spectra of the samples grown at different time are shown in Fig. 7. All of the spectra show two distinct peaks [Fig. 7(a)]. For the yellow-orange emission centered at 2.11 eV, the luminescent intensity keeps increasing until $t=6$ h and then decreases gradually when the time continually increase to 12 h [Fig. 7(c)]. For the UV emission (the enlarged image of the UV emission in Fig. 7(a) can be seen in Fig. 7(b), the intensity achieves the largest and the peak position has a 0.07 eV blueshift when $t=6$ h, thereafter, the intensity has a slight shake and the peak position redshift slowly [Fig. 7(d)]. In fact, the intensity of the emission is mainly determined by the degree of surface passivation. At the early stage of the hydrolysis of TEOS, only parts of $ZnS:Mn^{2+}$ NWs and ZnO QDs were encapsulated by the silica shell, while the rest of $ZnS:Mn^{2+}$ NWs and ZnO QDs still remained in the solution, which can be removed in the experiment. So, the surface of $ZnS:Mn^{2+}$ NWs and ZnO QDs can be passivated fully by ZnO QDs and SiO_2, respectively. With the increase in the hydrolysis time of TEOS, the silica shell became thick and more $ZnS:Mn^{2+}$ NWs and ZnO QDs would be encapsulated. But the thick ZnO and SiO_2 coating would induce strain at the interface caused by the lattice mismatch between each other. It would result in new traps for carriers, which are thought to be the main reason for the decrease in the yellow-orange and UV emission after $t=6$ h. It can be seen that the peak position of the yellow-orange emission does not change. Since the number of ZnO QDs on the surface of $ZnS:Mn^{2+}$ NWs can be estimated by the equation:

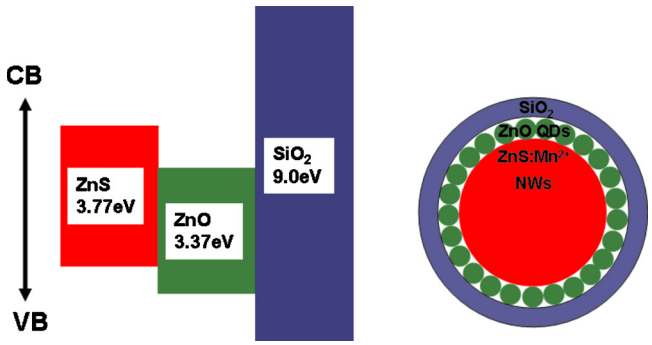

SCHEME 1. (Color online) Schematic diagram of bandgap and band offsets (in electron volt) for interfaces among $ZnS:Mn^{2+}$ NWs, ZnO QDs, and SiO_2.

$$N = \frac{2\pi(R+r)}{2r}L$$

where R and r is the radius of $ZnS:Mn^{2+}$ NWs and ZnO QDs, respectively, L is the length of the NWs. Assuming $L=1$, N is about 18. So, with the thickening of ZnO QDs, the residual stress on the interface does not change much due to the limited contact surface between $ZnS:Mn^{2+}$ NWs and ZnO QDs, resulting in the position of the yellow-orange unchanged. Since the structure of $ZnS:Mn^{2+}/ZnO@SiO_2$ nanocomposites behaves more like a type-I structure (Scheme 1), where the electron–hole recombination occurs mainly in the core, as they do not show the featureless subband-gap absorption tail implying the spatially indirect transitions expected for type-II structure.[40] So, the blueshift in the UV emission is caused by the covalently bonding between ZnO and SiO_2 when the shell is thin. With thickening the shell, the redshift in the UV emission can be ascribed to the partial leakage of the exciton into the SiO_2 matrix, which is commonly observed in the normal type-I core/shell systems.[41]

Figure 8(a) shows the temperature-dependent PL spectra of $ZnS:Mn^{2+}/ZnO@SiO_2$ nanocomposites recorded in the temperature range from 77 to 277 K. The enlarged UV emission in Fig. 8(a) can be seen in Fig. 8(b). As the temperature increased, the following features can be observed: (i) the intensity of the yellow-orange emission decreases, whereas the intensity of the UV emission increases from 77 to 257 K, and then decreases from 257 to 297 K, (ii) the photon energies of the yellow-orange and UV emission show a blueshift in about 25 meV and a redshift in about 73 meV, respectively, (iii) both of the yellow-orange and UV emission show a slight broaden, i.e., the full width at half-maximum (FWHM) increases.

Figure 9 shows the FWHM, photon energy, and intensity of the yellow-orange (green square line) and UV (red triangle line) emission as a function of temperature. As seen in Fig. 9(a), the slight increase in the FWHM as the temperature increases from 77 to 277 K for both the yellow-orange and UV emission can be observed, which can be explained by the electron–phonon coupling.[42,43] As seen in Figs. 8 and 9(b), the blueshift in the yellow-orange emission is likely due to the enhancement of the crystal field at lower temperatures caused by the crystal lattice contraction,[42,44] which is similar to the temperature behavior of the Mn^{2+} emission in bulk semiconductors.[45] Consequently, the emitting state, i.e., $^4T_1$ of Mn^{2+} shifts to lower energy with decreasing temperature.[44] For the UV emission, thermal expansion and electron–phonon interaction, in principle, contribute to the redshift when increasing temperature.[43] As seen in Fig. 9(c), the temperature dependence of the PL-integrated intensity clearly varies for the yellow-orange and UV emission. Generally, the PL intensity decreases with the increase in temperature and the temperature dependence satisfies the Arrhenius behavior as a consequence of temperature quenching effects. The anomalous enhancement of the PL intensity with the temperature for the UV emission may be caused by the spatially localized excitons on the surface. Since FT-IR and PL spectra have clearly proved the existence of abundant surface states on the nanocomposites surface. These surface states can trap many photogenerated carriers. The increasing temperature would make more trapped carriers obtain enough thermal energy to escape from the surface states, thereby increase the combination probability of the electrons and holes, and hence make the UV intensity increase. So, the density of the surface state can overrun the influence of temperature quenching and even alter the PL properties.

IV. CONCLUSIONS

In summary, $ZnS:Mn^{2+}$ NWs/ZnO QDs were encapsulated by a layer of mesoporous SiO_2 to form

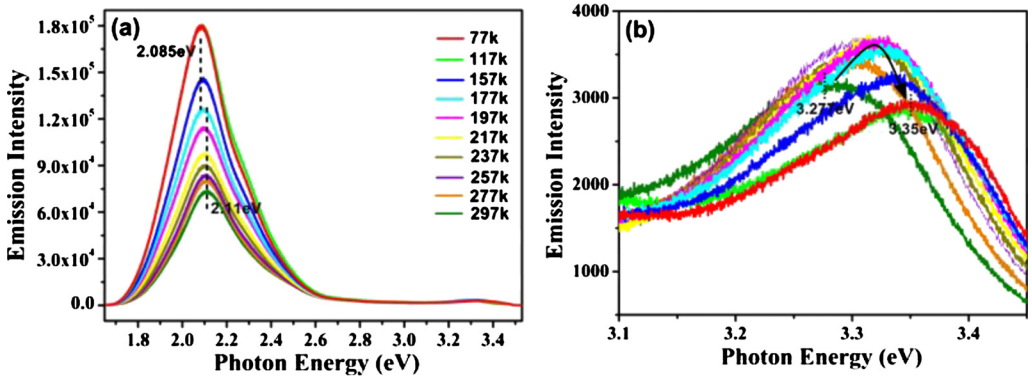

FIG. 8. (Color online) (a) Temperature-dependent PL spectra of $ZnS:Mn^{2+}/ZnO@SiO_2$ nanocomposites. (b) The enlarged image of the UV emission in Fig. 8(a).

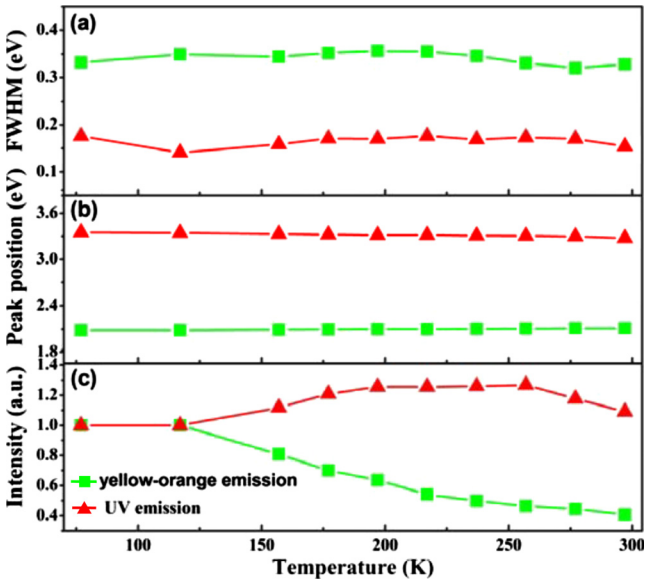

FIG. 9. (Color online) Temperature dependence of (a) the FWHM, (b) the peak energy, (c) the PL-integral intensity of the yellow-orange (green square) and UV (red triangle) emission. The integrated intensity of the yellow-orange and UV emission is normalized to the PL spectrum collected at 77 K.

$ZnS:Mn^{2+}/ZnO@SiO_2$ heterostructure. Due to the contributions of the visible emission by $ZnS:Mn^{2+}$ NWs and the ultraviolet emission by ZnO QDs, the heterostructures are biluminescent in nature. The PL intensity ratio of the dual emission can be tuned by regulating the hydrolysis time of TEOS. The mesoporous silica plays a key role in protecting the surface of the nanocomposites. The photon energies of the yellow-orange and UV emission exhibit blueshift and redshift as the temperature increased, respectively. The anomalous enhancement of the PL-integrated intensity for the UV emission with the temperature indicates that the high surface state density existing in ZnO QDs can overrun the influence of temperature quenching and even alter the PL properties. Therefore, we believe that this new $ZnS:Mn^{2+}/ZnO@SiO_2$ nanocomposites heterostructure would be the ideal biluminescent materials, which are more applicable for the fabrication of optoelectronic devices, such as UV light-emitting diodes, diode lasers and ultrasensitive ion probes.

ACKNOWLEDGMENTS

This work was financially supported by the National Natural Science Foundation of China (Grant Nos. 60778040, 60878039, and 10904050), National Programs for High Technology Research and Development of China (863) (Grant No. 2009AA03Z303), and Program for the development of Science and Technology of Jilin province (Grant No. 20082112).

[1]M. Y. Lu, J. H. Song, M. P. Lu, C. Y. Lee, L. J. Chen, and Z. L. Wang, ACS Nano **3**, 357 (2009).
[2]P. K. Santra, R. Viswanatha, S. M. Daniels, N. L. Pickett, J. M. Smith, P. O'Brien, and D. D. Sarma, J. Am. Chem. Soc. **131**, 470 (2009).
[3]M. W. Murphy, K. P. S. Grace, X. T. Zhou, J. G. Zhou, M. Coulliard, G. A. Botton, and T. K. Sham, J. Phys. Chem. C **113**, 4755 (2009).
[4]D. P. Wei, Y. Ma, H. Y. Pan, and Q. Chen, J. Phys. Chem. C **112**, 8594 (2008).
[5]S. Kar and S. Biswas, A. C. S. Appl. Mater. Interfaces **1**, 1420 (2009).
[6]Y. Song, X. Cao, Y. Guo, P. Chen, Q. Zhao, and G. Shen, Chem. Mater. **21**, 68 (2009).
[7]R. S. Yang, Y. L. Chueh, J. R. Morber, R. Snyder, L. J. Chou, and Z. L. Wang, Nano Lett. **7**, 269 (2007).
[8]Z. W. Quan, D. M. Yang, C. X. Li, D. Y. Kong, P. P. Yang, Z. Y. Cheng, and J. Lin, Langmuir **25**, 10259 (2009).
[9]Q. J. Sun, Y. A. Wang, L. S. Li, D. Y. Wang, T. Zhu, J. Xu, C. H. Yang, and Y. F. Li, Nat. Photonics **1**, 717 (2007).
[10]Y. Yang, Y.-Q. Li, and S.-Y. Fu, and H.-M. Xiao, J. Phys. Chem. C **112**, 10553 (2008).
[11]J. Yan, X. Fang, L. Zhang, Y. Bando, U. K. Gautam, B. Dierre, T. Sekiguchi, and D. Golberg, Nano Lett. **8**, 2794 (2008).
[12]X. Fan, M. L. Zhang, I. Shafiq, W. J. Zhang, C. S. Lee, and S. T. Lee, Adv. Mater. **21**, 2393 (2009).
[13]L. Yu, X. F. Yu, Y. Qiu, Y. Chen, and S. Yang, Chem. Phys. Lett. **465**, 272 (2008).
[14]K. M. Sulieman, X. Huang, J. Liu, and M. Tang, Smart Mater. Struct. **16**, 89 (2007).
[15]V. Wood, J. E. Halpert, M. J. Panzer, M. G. Bawendi, and V. Bulovic, Nano Lett. **9**, 2367 (2009).
[16]Y. Fang, S. Chu, H. Chen, P. Kao, I. Chen, and C. Hwang, J. Electrochem. Soc. **156**, K55 (2009).
[17]T. P. Surkova, V. R. Galakhov, and E. Z. Kurmaev, Low Temp. Phys. **35**, 79 (2009).
[18]R. N. Bhargava and D. Gallagher, Phys. Rev. Lett. **72**, 416 (1994).
[19]S. Biswas, S. Kar, and S. Chaudhuri, J. Phys. Chem. B **109**, 17526 (2005).
[20]J. Yang, X. Liu, L. Yang, Y. Wang, Y. Zhang, J. Lang, M. Gao, and B. Feng, J. Alloys Compd. **477**, 632 (2009).
[21]S. Kar, S. Santra, and H. Heinrich, J. Phys. Chem. C **112**, 4036 (2008).
[22]F. Li, X. Huang, Y. Jiang, L. Liu, and Z. Li, Mater. Res. Bull. **44**, 437 (2009).
[23]F. Gu, C. Z. Li, S. F. Wang, and M. K. Lu, Langmuir **22**, 1329 (2006).
[24]P. K. Sharma, R. K. Dutta, M. Kumar, P. K. Singh, and A. C. Pandey, J. Lumin. **129**, 605 (2009).
[25]Z. Li, W. Shen, L. Fang, and X. Zu, J. Alloys Compd. **463**, 129 (2008).
[26]S. K. Mandal, A. R. Mandal, S. Das, and B. Bhattacharjee, J. Appl. Phys. **101**, 114315 (2007).
[27]J. Finster, Surf. Interface Anal. **12**, 309 (1988).
[28]D. Sprenger, H. Bach, W. Meisel, and P. Gütlich, J. Non-Cryst. Solids **126**, 111 (1990).
[29]H. C. Ong and R. P. H. Chang, Appl. Phys. Lett. **79**, 3612 (2001).
[30]J. Y. Lao, J. Y. Huang, D. Z. Wang, and Z. F. Ren, Nano Lett. **3**, 235 (2003).
[31]N. Pradhan and S. Efrima, J. Phys. Chem. B **108**, 11964 (2004).
[32]M. V. Limaye, S. Gokhale, S. A. Acharya, and S. K. Kulkarni, Nanotechnology **19**, 415602 (2008).
[33]K. Sooklal, B. S. Cullum, S. M. Angel, and C. J. Murphy, J. Phys. Chem. **100**, 4551 (1996).
[34]L. Yang, J. Yang, X. Liu, Y. Zhang, Y. Wang, H. Fan, D. Wang, and J. Lang, J. Alloys Compd. **463**, 92 (2008).
[35]Y. W. Chen, Q. Qiao, Y. C. Liu, and G. L. Yang, J. Phys. Chem. C **113**, 7497 (2009).
[36]D. Jiang, L. Cao, W. Liu, G. Su, H. Qu, Y. Sun, and B. Dong, Nanoscale Res. Lett. **4**, 78 (2009).
[37]Y. M. Niquet, G. Allan, C. Delerue, and M. Lannoo, Appl. Phys. Lett. **77**, 1182 (2000).
[38]M. S. Sander, R. Gronsky, Y. M. Lin, and M. S. Dresselhaus, J. Appl. Phys. **89**, 2733 (2001).
[39]Y. F. Zhu, D. H. Fan, and W. Z. Shen, J. Phys. Chem. C **112**, 10402 (2008).
[40]W. Zhang, G. Chen, J. Wang, B. C. Ye, and X. Zhong, Inorg. Chem. **48**, 9723 (2009).
[41]Z. Fang, Y. Li, H. Zhang, X. Zhong, and L. Zhu, J. Phys. Chem. C **113**, 14145 (2009).
[42]W. Chen, F. Su, G. Li, A. G. Joly, J. O. Malm, and J. O. Bovin, J. Appl. Phys. **92**, 1950 (2002).
[43]R. Muñoz-Espí, G. Jeschke, I. Lieberwirth, C. M. Gómez, and G. Wegner, J. Phys. Chem. B **111**, 697 (2007).
[44]W. Chen, V. F. Aguekian, N. Vassiliev, A. Y. Serov, and N. G. Filosofov, J. Chem. Phys. **123**, 124707 (2005).
[45]F. H. Su, B. S. Ma, Z. L. Fan, K. Ding, G. H. Li, and W. Chen, J. Phys.: Condens. Matter **14**, 12657 (2002).